Bone Tumors: MRI Pitfalls

31

Remide Arkun and Mehmet Argin

Contents

R. Arkun, MD (✉) • M. Argin, MD
Department of Radiology, Ege University Medical School, 35100, Bornova/Izmir, Turkey
e-mail: rarkun@yahoo.com; remide.arkun@ege.edu.tr; margin35@yahoo.com

Abbreviations

CT	Computed tomography
MRI	Magnetic resonance imaging

31.1 Introduction

Bone tumors are a relatively infrequent finding in musculoskeletal radiology, and malignant bone tumors are far less common than benign ones. The incidence of bone sarcoma is estimated to be 0.2% of the overall human tumor burden. A wide range of musculoskeletal tumors and tumor-like conditions may be encountered when patients undergo radiological examinations. The imaging features of certain normal, reactive, benign neoplastic, inflammatory, traumatic, and degenerative processes in the musculoskeletal system may mimic malignant tumors. Misinterpretation of the imaging findings can lead to inappropriate clinical management of the patient. Tumor-like lesions also can show similar imaging findings to benign and malignant bone tumors. Radiography is accepted as the single most valuable imaging modality in the diagnosis of bone lesions. Although the differential diagnosis of primary bone tumor remains based on their radiographic appearances, evaluation of bone tumors involves a multimodality approach, and cross-sectional imaging has extraordinarily improved the ability to characterize tumors.

W.C.G. Peh (ed.), *Pitfalls in Musculoskeletal Radiology*, DOI 10.1007/978-3-319-53496-1_31

Magnetic resonance imaging (MRI) is the most sensitive and accurate imaging technique for evaluation of musculoskeletal tumors. MRI demonstrates the depth, size, and local extent of tumors. Published opinions regarding the value of MRI in characterizing the pathological nature of musculoskeletal masses and discriminating between benign and malignant lesions are divergent, with different papers showing that specificity values of MRI range from 76% to 90%. There are also opposing reports that MRI has low specificity in differentiation between benign and malignant masses, and most lesions demonstrate a nonspecific appearance. Besides benign and malignant bone tumors, there are numerous non-tumoral entities which have similar morphologic and signal changes and can mimic the imaging findings of bone tumors.

A large number of these lesions clearly have the characteristic findings of nonneoplastic entities and do not need further workup. The remainder of non-tumoral and tumor-like lesions needs management that includes close collaboration with orthopedic oncologists and further investigation such as biopsy or surgery. In the evaluation of bone tumors with MRI, the radiologist should be familiar with the imaging findings of non-tumoral and tumor-like lesions which will cause confusion. This chapter aims to highlight some pitfalls, including normal variants, congenital and traumatic disorders, and tumor-like disease of bone, which may mimic MRI findings of bone tumors.

31.2 Normal Hematopoietic Bone Marrow

Bone marrow is one of the largest organs in the body, after the osseous skeleton, skin, and body fat, and the marrow cavity of the skeleton contains both fat and hematopoietic cells. The normal composition and distribution of bone marrow change with age and affect the MRI signal appearances of marrow. Because metastatic and primary hematologic malignancies commonly involve the bone marrow, knowledge of the normal distribution of red and yellow marrow and variances is of primary necessity for correct interpretation. On gross examination, bone marrow appears red (hematopoietic marrow) or yellow (fatty marrow), depending on its predominant components. Normal red marrow has lower signal intensity than that of fat and generally equal or higher signal intensity than that of skeletal muscle on T1-weighted MR images. Normal yellow marrow has similar signal intensity to subcutaneous fat on T1-weighted MR images and appears darker on T2-weighted MR images obtained with fat suppression. On fat-suppressed T2-weighted MRI, the signal intensity of normal red marrow is higher than that of yellow marrow and is often similar to or slightly higher than that of skeletal muscle (Vogler and Murphy 1988; Hwang and Panicek 2007).

At birth, hematopoietic marrow is present throughout the entire skeleton, but various regions of hematopoietic marrow then start converting to fatty marrow. The transition occurs over two decades in a predictable sequence, beginning in the periphery of the skeleton and extending in a symmetrical centripetal manner into the central skeleton and from diaphyseal to metaphyseal regions in the long bones. Following attainment of an adult pattern, the fractional balance of red and yellow marrow contained within axial and proximal long bones may slowly change with advancing age (Vogler and Murphy 1988; Hwang and Panicek 2007; Howe et al. 2013). This appearance is usually appreciated on shoulder and hip MRI examinations. Although the distal appendicular skeleton usually has a uniform distribution of yellow marrow in adults, increased residual red marrow can be seen within the distal femur in knee MRI of patients who are heavy smokers, marathoners, and obese females of menstruating age. Knowledge of the typical distribution of residual red marrow in adults and the signal characteristics of normal red marrow should allow the avoidance of misdiagnosis.

The signal intensity, morphology, and distribution of marrow also can help to distinguish such normal variations from marrow lesions (Fig. 31.1). Marrow metastases usually have lower signal intensity than that of muscle and tend to be more rounded with sharply defined borders, whereas foci of red marrow also can often be recognized by their poorly defined

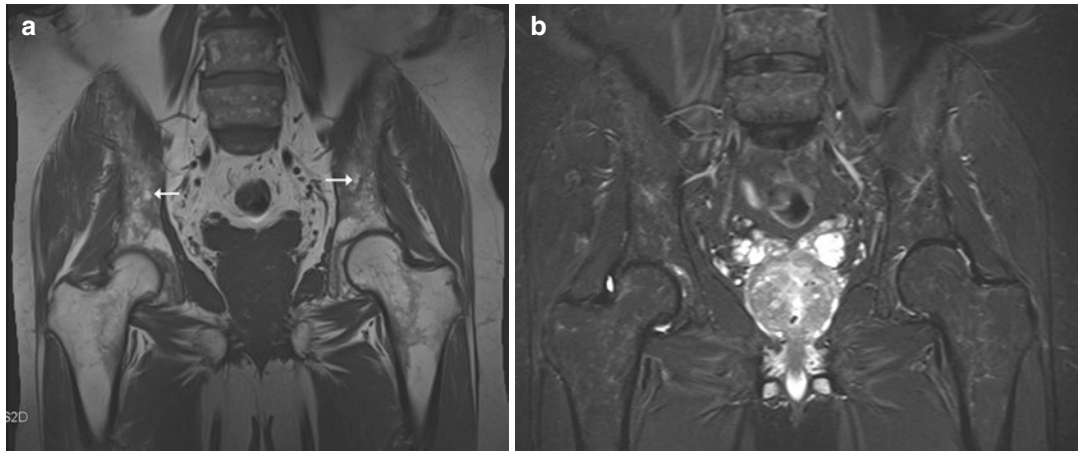

Fig. 31.1 Bone marrow reconversion in a 66-year-old man who is a heavy smoker. (**a**) Coronal T1-W MR image of the pelvis shows heterogeneous intermediate to hypointense signal in both iliac bones with focal hyperintense residue fatty marrow (*arrows*). There is a similar appearance in the L4 and L5 vertebral bodies. Note patchy intermediate signal changes due to residual red marrow on both medial aspects of the femoral neck. (**b**) The corresponding coronal STIR MR image of the pelvis shows diffuse, slightly more hyperintense signal than that of skeletal muscle in the L4 and L5 vertebral bodies and both iliac bones. There is no abnormal focal signal hyperintensity to suggest tumoral infiltration

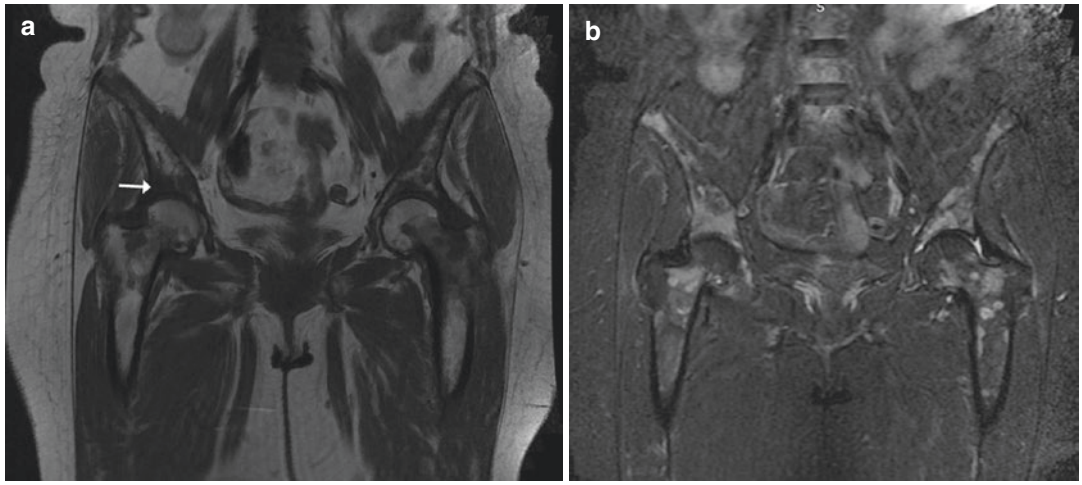

Fig. 31.2 Breast carcinoma metastases in a 55-year-old woman. (**a**) Coronal T1-W MR image of the pelvis shows areas of heterogeneous hypointense signal in both iliac bones and femoral necks. Signal intensity is lower than that of the muscle at the right acetabular roof (*arrow*). (**b**) The corresponding coronal STIR MR image of the pelvis shows heterogeneous hyperintense signal in both iliac bones. There are also rounded hyperintense foci in both femoral necks

feathery margins that interdigitate with fatty marrow on T1-weighted MR images, as well as by its asymmetrical distribution. On fluid-sensitive MRI sequences, metastatic lesions have higher signal intensity than that of normal hematopoietic red marrow (Howe et al. 2013; Arkun and Argin 2014) (Fig. 31.2).

31.3 Melorheostosis

Melorheostosis is an uncommon, nonhereditary, benign, sclerosing mesodermal disease that affects the skeleton and adjacent soft tissues, with an incidence of 0.9 cases per million. Appendicular skeleton involvement is more

common than the axial skeleton. The periosteal hyperostosis along the cortex of long bones, resembling the dripping or flowing of candle wax, gives the condition its name, which is derived from Greek. Besides bone changes, para-articular soft tissue masses, intra-articular extensions, and spinal involvement have been described. Cross-sectional imaging techniques are useful to reveal manifestation of the disease and allow differentiation from other disease and malignancy. The characteristic radiographic appearance is that of flowing cortical hyperostosis along one side of the shaft of the long bone resembling "melting wax flowing down the side of a candle." However, it can be seen as an osteoma-like appearance or can be seen together with complete bony obliteration of bone marrow, bony overgrowth, or paraosseous soft tissue ossifications.

On MRI, due to cortical hyperostosis, signal hypointensity is seen on all pulse sequences, with encroachment on marrow space resulting from endosteal involvement. Intramedullary focal signal hyperintensity on T2-weighted MR images is a very rare finding. If there is a para-articular soft tissue mass, the MRI appearance of a soft tissue mass is variable, and heterogeneous signal intensity due to mineralized areas, fat-containing areas, and fibrovascular tissue may be seen (Fig. 31.3). This can mimic parosteal osteosarcoma, and computed tomography (CT) is helpful to demonstrate the cleft in between the bone and the soft tissue mass (Azouz and Greenspan 2005; Suresh et al. 2010).

31.4 Traumatic Disorders

31.4.1 Stress Fracture

Bone marrow edema may result from a variety of nonneoplastic disorders. Although stress fracture is one of the common causes of bone marrow edema, it is a diagnostic challenge in skeletal imaging. The term "stress fracture" refers to the failure of the skeleton to withstand submaximal forces over time. Two forms of stress fracture have been defined, namely, fatigue fracture which occurs in normal bone placed under the stress of a new or abnormal activity and insufficiency fractures which are the result of normal activities on bones of abnormal or deficient bone mineral (Fayad et al. 2005; Wall and Feller 2006; Arkun and Argin 2014). However, in the literature, the term stress fracture has generally been used, instead of fatigue fracture (Arkun and Argin 2014).

Although radiography is the first imaging technique for bone lesions, stress fractures are usually not visible radiographically at the time of initial presentation. Radiographs are positive in only 10–25% of cases at the initial presentation; and 2–12 weeks after injury, radiographs can be still normal in up to 33–50% of cases. If a stress fracture is visible on radiographs, cortical resorption, periosteal reaction, cortical thickening, endosteal sclerosis, and sclerotic line perpendicular to the trabeculae are typical imaging findings. For a patient who has extremity pain, with or without swelling and tenderness, and does not have a clear history of trauma or chronic overuse type of activity and normal radiographs, there is necessity for another imaging technique.

MRI typically shows periosteal and bone marrow edema without a visible fracture line in the early phase of the disease. There may be a variable degree of surrounding soft tissue edema. Enhancement of the marrow and surrounding soft tissues may be seen after contrast administration, mimicking other disease such as infection or tumor (Fig. 31.4). A hypointense fracture line, which is seen as a linear area of hypointense signal, with surrounding ill-defined T2-hyperintense signal (edema) on fluid-sensitive sequences, allows an accurate diagnosis of stress fractures (Fayad et al. 2005; Gould et al. 2007; Arkun and Argin 2014). Stacy and Dixon (2007) stated that the edema associated with stress fracture is frequently much more pronounced on fat-suppressed T2-weighted images than on T1-weighted MR images and is often ill-defined, particularly on T1-weighted images. In contrast, a well-defined hypointense rounded lesion is usually evident on T1-weighted images in patients with a neoplasm.

Insufficiency fractures occur more commonly in the elderly and, in particular, patients with

Fig. 31.3 Melorheostosis in a 40-year-old woman with right shoulder pain. (**a**) Right humerus radiograph, including the shoulder joint and right hemithorax, shows flowing cortical hyperostosis along the medial shaft of the humerus (*open arrow*). There is also paraosseous soft tissue ossification in the right axilla and parasternal region (*arrows*). (**b**) Contiguous coronal T1-W MR images of the humerus show markedly hypointense flowing cortical hyperostosis (*open arrows*) and a heterogeneous irregular mass adjacent to the proximal metaphysis of the humerus (*black arrows*). The lesion has areas of signal void due to mineralization. (**c**) Axial fat-suppressed T2-W MR image shows markedly hypointense intramedullary involvement and a heterogeneous irregular mass adjacent to the bone (*arrows*). Note that there is no continuity between the cortical bone and the soft tissue mass. (**d**) Coronal contrast-enhanced fat-suppressed T1-W MR image shows enhancement of the soft tissue mass (*arrow*)

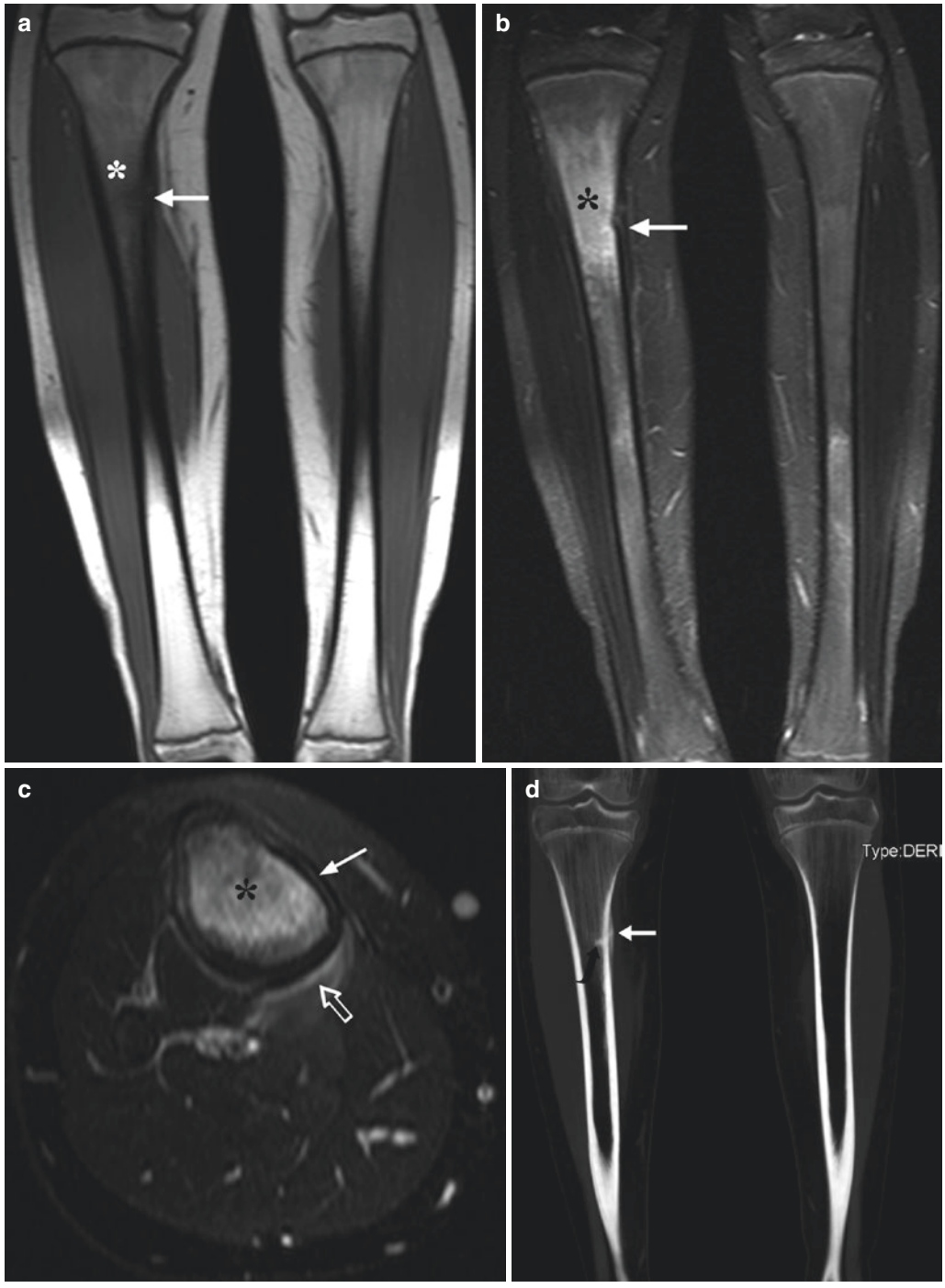

Fig. 31.4 Stress fracture in a 13-year-old boy with right leg pain. (**a**) Coronal T1-W MR image of the lower extremities shows an area of hypointense bone marrow signal in the proximal metaphysis of the right tibia (*black asterisk*) and cortical thickening at the medial cortex of the right tibia (*white arrow*). (**b**) The corresponding coronal fat-suppressed T2-W MR image shows an area of hyperintense signal due to bone marrow edema (*black asterisk*) and cortical thickening due to periosteal reaction (*arrow*). (**c**) Axial contrast-enhanced fat-suppressed T1-W MR image shows enhancement of the bone marrow (*black asterisk*), periosteal reaction (*arrow*), and soft tissue edema (*open arrow*). (**d**) The fracture line (*black curved arrow*) with solitary periosteal reaction (*white arrow*) is better delineated on the coronal reformatted CT image

cancer. These patients can be detected incidentally during MRI or CT examinations which are performed for other reasons. Several pathological conditions which include postmenopausal osteoporosis, corticosteroid-induced osteoporosis, radiation therapy, rheumatoid arthritis, Paget disease of bone, renal osteodystrophy, and long-standing bed rest may decrease bone resistance and predispose the development of insufficiency fractures (Fayad et al. 2005; Cabarrus et al. 2008; Arkun and Argin 2014). The most common locations are the pelvic girdle including the sacrum, proximal femur, and vertebral bodies, particularly the lumbar and lower thoracic spine. Patients typically present with acute pain, depending on the site of the fracture. Because of the nonspecific clinical presentation, imaging has an important role in the detection and diagnosis of insufficiency fractures.

Frequently, these fractures are radiographically occult, and some of these fractures, in particular sacral insufficiency fractures, are relatively underdiagnosed. If an insufficiency fracture is visible on radiographs, common findings include a sclerotic band or line, bone expansion, and exuberant callus. The lytic fracture line or cortical break is rarely observed. If the radiologist is not aware of this appearance, particularly in setting of existing malignant disease, insufficiency fracture may be misdiagnosed as bone metastasis (Cabarrus et al. 2008; Krestan et al. 2011). Sacral insufficiency fractures can be associated with insufficiency fractures of the pubic rami and parasymphyseal region. Early diagnosis is best made with bone scintigraphy or MRI. Although bone scintigraphy is highly sensitive, it relies on accurate interpretation of the uptake pattern, and atypical uptake patterns may be difficult to interpret. In bilateral sacral insufficiency fractures, H-shaped (Honda sign) increased activity or the combination of concomitant sacral and parasymphyseal uptake is considered a typical finding of insufficiency fractures (Campbell and Fajarda 2008; Krestan et al. 2011).

MRI is as sensitive as bone scintigraphy but is of higher specificity, both in isolating the exact anatomical location and in distinguishing fractures from tumors or infection. Moreover, MRI is the most sensitive imaging technique in the early stage of insufficiency fracture (Cabarrus et al. 2008; Campbell and Fajardo 2008; Krestan et al. 2011). MRI shows hypointense signal on T1-weighted images and hyperintense signal on T2-weighted images. In the sacrum, linear bands are seen within the sacral ala and body, with the bands being parallel to the sacroiliac joints (Fig. 31.5). Although on MRI, signal hyperintensity and a hypointense fracture line within the area of edema are characteristic findings, a hypointense fracture line is not seen in 7% of cases. The benefit of Gadolinium-based contrast agent administration is controversial and is not commonly applied. Radiologists should be familiar with imaging findings of insufficiency fractures because malignant lesions are frequently suspected in patients who have undergone radiation therapy and chemotherapy of the pelvis (Cabarrus et al. 2008; Lyders et al. 2010). It has been reported that ill-defined signal hypointensity on T1-weighted images is significantly more likely to represent insufficiency fractures, while adjacent muscle signal abnormality reflects pathological fracture (Campbell and Fajardo 2008). Occasionally, MRI can be confusing, especially if a fracture line is not evident, and correlative CT or follow-up imaging may be useful (Cabarrus et al. 2008; Lyders et al. 2010).

31.4.2 Avulsion Fracture

An avulsion fracture is one that occurs when a joint capsule, ligament, or muscle insertion or its origin is pulled off from the bone as a result of a sprain, dislocation, or strong contracture of the muscle against resistance. As the soft tissue is pulled away from the bone, a bony fragment (or fragments) remains attached to the soft tissue. It is usually seen among athletes and most commonly occurs at the pelvis, shoulder, elbow, knee, ankle, and foot. In a basic avulsion fracture, radiographs of the site reveal that a small piece of bone has been torn away. Physical findings, symptoms, the patient's age, and biomechanical analysis of the accident can collectively raise the suspicion of an avulsion fracture, and conventional radiography

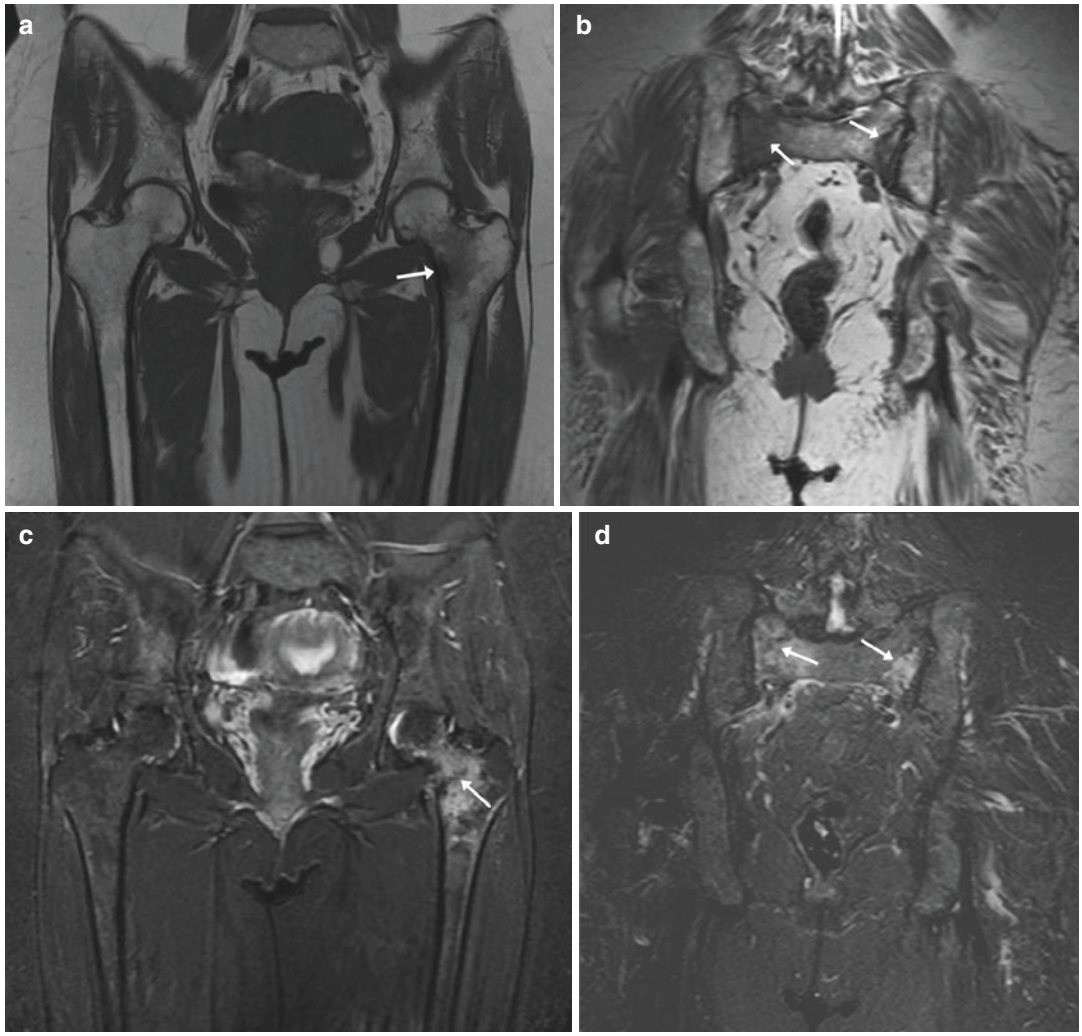

Fig. 31.5 Multiple insufficiency fractures in a 75-year-old woman. (**a**, **b**) Contiguous coronal T1-W MR images of the pelvis show an area of signal hypointensity in the left femoral neck (*arrow* in **a**) and right sacral ala (*arrow* in **b**) and a hypointense linear band that is located in the left sacral ala (*arrow*). (**c**, **d**) Contiguous coronal STIR MR images of the pelvis show hypointense fracture lines surrounded by bone marrow edema adjacent to the medial cortex of the left femoral neck (*arrow* in **c**) and within the sacral ala bilaterally (*arrows* in **d**)

can confirm the diagnosis, especially in long bones. In adolescents, because of inherent weakness of the apophysis, avulsion fracture is seen together with musculotendinous junction injuries. In the pelvis, avulsion injuries usually occur before closure of the apophysis as a result of trauma. Among six sites, the ischial tuberosity is the most common site for pelvic avulsion injury.

A clinical history of sudden onset of severe pain at the site of avulsion is common in acute injury. Diagnosis can be achieved by clinical examination together with radiographs, and MRI or CT, as determined by availability. In case of a displaced fracture fragment, this is seen at the origin or insertion of a muscle or tendon. If an apophyseal avulsion is non-displaced or when the apophysis is unossified, radiographs can be negative. MRI will show hematoma, bone marrow edema, and periosteal stripping at the tendinous attachment sites (Stevens et al. 1999) (Fig. 31.6). In the healing phase, avulsion fractures can have an aggressive appearance with a protuberant mass and resemble an infectious or malignant process. Young adults with pelvic

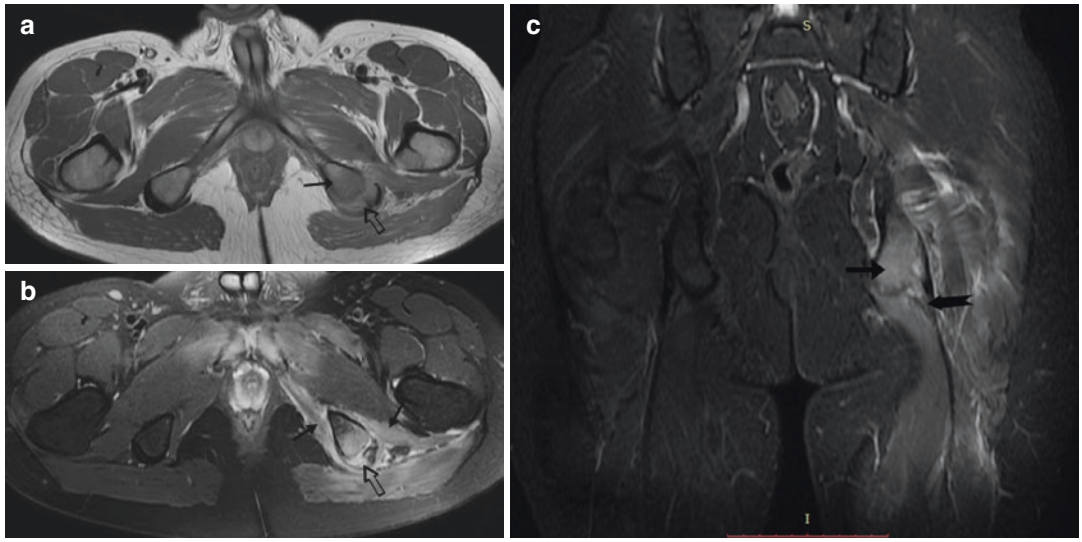

Fig. 31.6 Avulsion fracture in a 22-year-old male soldier who had pain in his left hip with walking difficulty. (**a**) Axial T1-W MR image of the pelvis shows an area of hypointense signal in the left ischium (*black arrow*) and hyperintense signal and separation of ischial tuberosity (*open black arrow*). (**b**) The corresponding axial fat-suppressed T2-W MR image shows muscle edema in the quadratus femoris and obturator internus muscles (*black arrows*). There is also hyperintense signal due to hematoma at the ischial tuberosity (*open black arrow*). (**c**) Coronal fat-suppressed T2-W MR image shows bone marrow edema in the ischium (*arrow*) and an area of signal hyperintensity due to musculotendinous junction injury at the proximal insertion of hamstrings (*closed arrow*) and extensive hamstring muscle edema

avulsion injuries can especially be mistaken as having a malignant tumor due to an aggressive appearance caused by exuberant bone marrow and soft tissue edema. CT will nicely identify any present bone fragments and delineate findings associated with healing (Gould et al. 2007; Arkun and Argin 2014).

31.5 Erdheim-Chester Disease

Erdheim-Chester disease (ECD) is a rare non-familiar disorder, first described by Jakob Erdheim and William Chester in 1930 as "lipid granulomatosis". Until now, approximately 500 cases had been reported in the literature. The clinical manifestations of ECD are nonspecific and depend on the affected organ. It may be asymptomatic, clinically indolent, or, sometimes, life threatening. Bone involvement is almost universal in ECD (96% of cases), and more than 50% of cases have at least one site of associated extra-skeletal involvement, such as the kidney, skin, central nervous system, or heart. Patients may have bone pain, frequently juxta-articular at the knees and ankles. In long bones, ECD is characterized by bilateral symmetrical sclerosis of the diametaphyseal regions of long bones and infiltration of foamy lipid-laden histiocytes. This may be difficult to diagnose because it is rarely seen and has a broad spectrum of clinical manifestations.

The diagnosis is based on radiological findings of striking patchy medullary sclerosis in the diametaphyseal region, which is mostly confined to the appendicular skeleton in a symmetrical fashion. Radiographs show bilateral and symmetrical cortical osteosclerosis of the diaphyseal and metaphyseal regions of the long bones, with a clear-cut limit between the involved portion of the bone and the epiphyseal region, which is usually spared. Rarely, these alterations may be associated with periostitis and endosteal thickening. On MRI, skeletal involvement consists of extensive replacement of the fatty marrow by hypointense signal on T1-weighted images, heterogeneous signal on T2-weighted/STIR images, and enhancement after gadolinium injection (Fig. 31.7). MRI is useful to evaluate the extent of medullary bone disease and

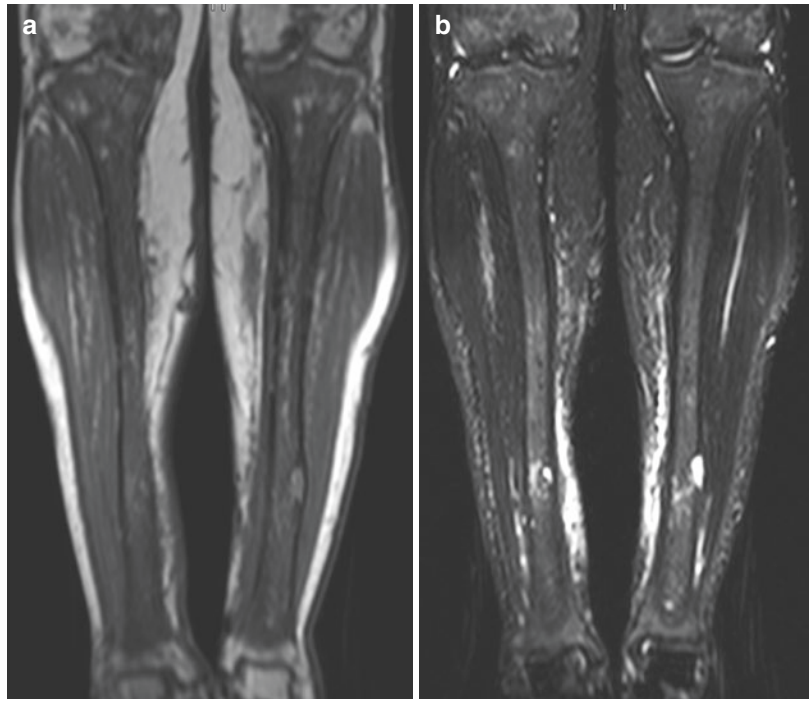

Fig. 31.7 Erdheim-Chester disease proven by bone biopsy in a 60-year-old woman who had bilateral knee pain. (**a**) Coronal T1-W MR image of the lower extremities shows extensive replacement of fatty marrow with areas of signal hypointensity bilaterally. Note that the distal epiphyses of both tibias are spared. (**b**) The corresponding coronal STIR MR image shows symmetrical heterogeneous signal hypointensity with cystic changes at the distal diaphysis of both tibias

diagnose the presence of associated osteonecrosis. Partial epiphyseal involvement can be seen on MRI. Symmetrical involvement almost excludes diseases such as osteomyelitis, Paget disease, lymphoma, and sclerotic sarcoidosis (Eyigor et al. 2005; Dion et al. 2006; Antunes et al. 2014).

31.6 Nora Lesion (Bizarre Parosteal Osteochondromatous Proliferation)

This entity is also known as bizarre parosteal osteochondromatous proliferation (BPOP) and may be mistaken for a surface or central osteosarcoma in the peripheral skeleton or in the long bones. Even if it is considered a reactive process, chromosomal abnormalities have been described, suggesting the possibility of a neoplasm. There is no gender predominance, and it is more common in the second and third decades of life. Although the classical location is on the surfaces of the small bones of hand and feet, 25% of cases are located in long bones, especially the radius and humerus. Radiographically, there is a heterotopic, well-defined calcified or ossified mass attached to cortical surface of bone. The mass can be pedunculated or sessile. There is no continuity between the lesion and cortex and medulla of host bone and no contact with the growth plate. On MRI, Nora lesion shows variable signal intensity on T1-weigheted images. It may show hyperintense signal on fluid-sensitive sequences and/or edema in the bone marrow and surrounding soft tissues and mild heterogeneous enhancement after gadolinium injection (Fig. 31.8). CT is more helpful than MRI in providing a better delineation of the relationship between the lesion and the host bone (Dhondt et al. 2006; Kershen et al. 2012; Rapppaort et al. 2014; Olvi et al. 2015b).

31.7 Fibrous Dysplasia

Rather than being a true neoplasm, fibrous dysplasia (FD) is a developmental anatomy of bone in which the normal medullary space is replaced by fibro-osseous tissue and small spicules of woven bone. FD may present in either monostotic (70–85%) or polyostotic (15–30%) forms. Although any bone within the skeleton can be affected, the tibia, proximal femur, pelvis, ribs,

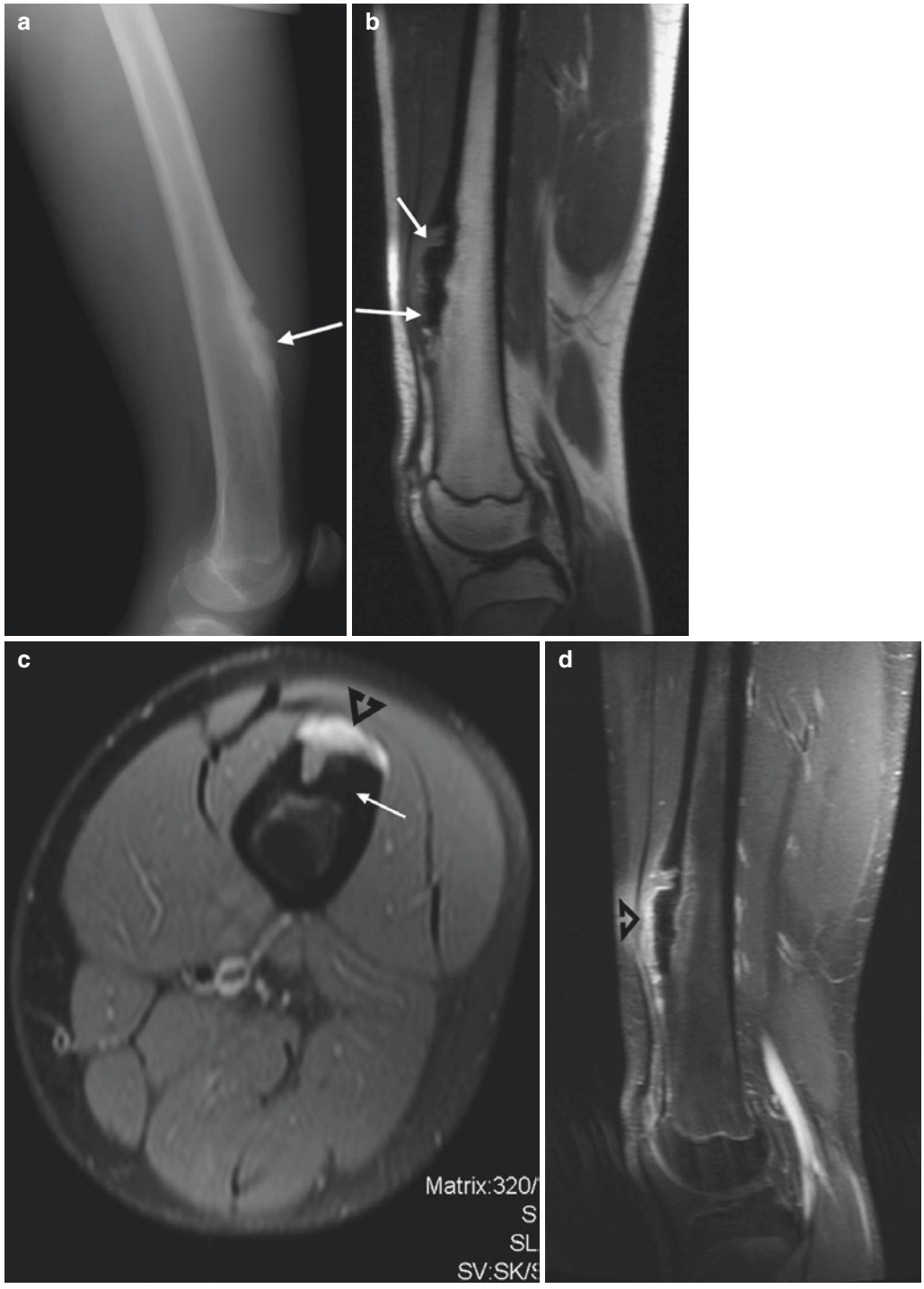

Fig. 31.8 Nora lesion in a 16-year-old boy with distal left thigh pain. (**a**) Left femur radiograph shows a sessile protuberant ossified mass attached to the anterior cortex of the left femur (*arrow*). (**b**) Sagittal T1-W MR image of the femur shows a sessile protuberant hypointense mass with a soft tissue component which has intermediate signal intensity located in the distal diaphysis of the femur (*arrows*). (**c**) Axial fat-suppressed T2-W MR image shows an ossified mass attached to the anterior cortex (*white arrow*) with a hyperintense soft tissue component (*open black arrow*) due to cartilage component. There is no continuity in between the lesion and medullary bone. (**d**) There is marked peripheral enhancement of the lesion on the sagittal contrast-enhanced fat-suppressed T1-W MR image (*open black arrow*)

and skull are the most common locations. It is usually located in the metadiaphysis, and radiographically, the most characteristic finding is a "ground-glass" radiolucent appearance within the bone. Other classical radiological findings include mild bony expansion with or without sclerosis, cortical thinning, and endosteal scalloping. Epiphyseal involvement is unusual, particularly before closure of the growth plate. Cortical destruction, soft tissue component, and any type of periosteal reaction are not seen, if there is no fracture. When the radiological appearance is typical and the patient is asymptomatic, further imaging is unnecessary. CT and MRI will show a solid heterogeneous lesion with possible cystic components.

On MR imaging, FD has signal hypointensity on T1-weighted images and variable signal intensity due to T2-weighted images. Lesions tend to be relatively homogeneous, unless complicated by fracture or secondary aneurysmal bone cyst. A peripheral hypointense rim corresponds to marginal sclerosis on radiographs. As the lesion matures, foci of hypointense signal appear that corresponds histologically to hypercellular fibrous tissue and hemosiderin deposits. This heterogeneous signal intensity and prominent bony expansion may simulate malignancy (Fig. 31.9). After gadolinium administration, variable enhancement can be seen, due to cystic and solid parts of the lesion. Adjacent marrow edema is generally absent in uncomplicated lesions.

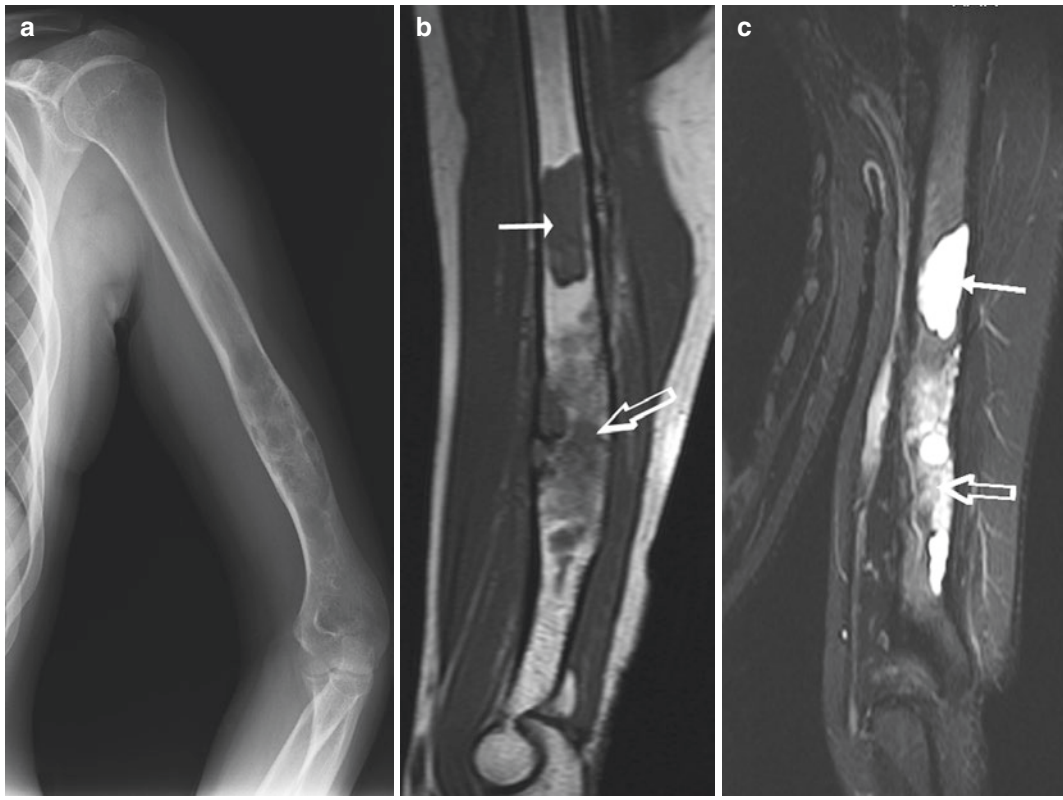

Fig. 31.9 Fibrous dysplasia in an 18-year-old girl with left arm pain. (**a**) Left humerus radiograph shows an expansile osteolytic lesion with well-defined margins, cortical thinning, and characteristic "ground-glass" appearance at the distal diaphyseal region. (**b**) Sagittal T1-W MR image shows different imaging findings in the humerus. There is bony expansion and heterogeneous hypointense signal area (*open arrow*) at the distal part of the lesion and a well-defined hypointense lesion at the proximal part of the lesion (*arrow*) (**c**) Coronal STIR MR image shows the lesion to have heterogeneous intermediate signal (*open arrow*) and cystic changes (*arrow*) with well-defined hypointense margins

Differential considerations may include unicameral bone cyst, non-ossifying fibroma (NOF), enchondroma, eosinophilic granuloma, aneurysmal bone cyst, myeloma, or metastatic disease, depending on location, patient age, and imaging appearances. Fibrous dysplasia may rarely undergo malignant transformation, with reported prevalence of 0.5% (Smith and Kransdorf 2000; Alyas et al. 2007; Arkun and Argin 2014).

31.8 Fibroxanthoma

The term "fibroxanthoma" is a common definition encompassing non-ossifying fibroma (NOF), fibrous cortical defect (FCD), and benign fibrous histiocytoma (BFH). All these lesions are a histologically identical benign fibrous neoplasm in the metaphysis of growing bones. It is one of the most frequent tumor-like lesions of bone and is more frequent in males (60%) than in females (40%). The historical division between FCD and NOF has been defined by size and natural history. FCDs are small metaphyseal cortical defects that disappear spontaneously (most common), whereas NOFs persist over time and may demonstrate interval growth into adulthood. It is located in the metaphyseal or metadiaphyseal area of long bones, and the most common locations are the distal femur and distal or proximal tibia, usually at the posteromedial surface. The long axis of the lesion is usually parallel to that of the host bone.

Radiographic findings of fibroxanthoma are typical and are seen as an eccentric ovoid osteolytic lesion of the metaphysis (or diametaphysis) arising close to the physeal plate, with a scalloped contour and well-demarcated sclerotic margins. Larger and multiple lesions can create confusion, when they are found incidentally on MRI which have been obtained for another reason in cancer patients. On MRI, NOF has hypointense and heterogeneous signal intensity on T1- and T2-weighted images related to its fibrous content, with a well-limited scalloped contour (Fig. 31.10). Areas of hyperintense signal due to microfractures or occult fractures may be seen on fat-suppressed T2-weighted images, and there is intense enhancement after gadolinium injection (Smith and Kransdorf 2000; Alyas et al. 2007; Arkun and Argin 2014).

31.9 Unicameral (Simple) Bone Cyst

Unicameral (or simple) bone cyst is an intramedullary, usually unilocular, cystic cavity filled with serous or serosanguineous fluid and lined by a membrane of variable thickness. Unicameral bone cyst is mostly seen in the first decades of life, which accounts for 80% of cases. The most common locations are the metaphysis of proximal humerus, proximal femur, and proximal tibia. The ilium, calcaneus, and talus are often affected in older patients. There is a centrally and symmetrically expanded osteolytic lesion with well-defined margins located at the metaphysis of long bones on radiographs. Epiphyseal involvement is uncommon. A multilocular or trabeculated appearance may be seen, due to prominent endosteal bony ridges in the inner cortical wall. When unicameral bone cyst is complicated by fracture, there may be small "fallen fragment" sign that has migrated and found floating in the fluid. There is no periosteal reaction except at sites of fracture.

Uncomplicated unicameral bone cysts have hypointense signal on T1-weighted images and hyperintense signal on T2-weighted MR images. Lesions that have a pathological fracture have heterogeneous signal intensities on both T1- and T2-weighted images, because of bleeding within the cyst. After gadolinium injection, they demonstrate enhancement with focal thick peripheral, heterogeneous, or subcortical patterns (Fig. 31.11). Septations within the lesions may be observed on MRI which may not be visualized on radiographs. Uncomplicated lesions are diagnosed easily on MRI. Lesions complicated by pathological fractures may reveal areas of heterogeneous signal and irregular enhancement patterns after the contrast administration. Differential considerations may include aneurysmal bone cyst, fibrous dysplasia, NOF, eosinophilic granuloma, and enchondroma (Mascard et al. 2015; Olvi et al. 2015a).

Fig. 31.10 Non-ossifying fibroma in a 17-year-old girl. (**a**) Left femur radiograph shows a lobulated intramedullary ossified lesion at the distal metadiaphyseal area of the bone (*arrows*). (**b**) Coronal, (**c**) sagittal, and (**d**) axial T1-W MR images show that the lesion has lobulated margins and heterogeneous signal intensity and the relationship of the lesion with the posterior endosteal cortex (*arrows*)

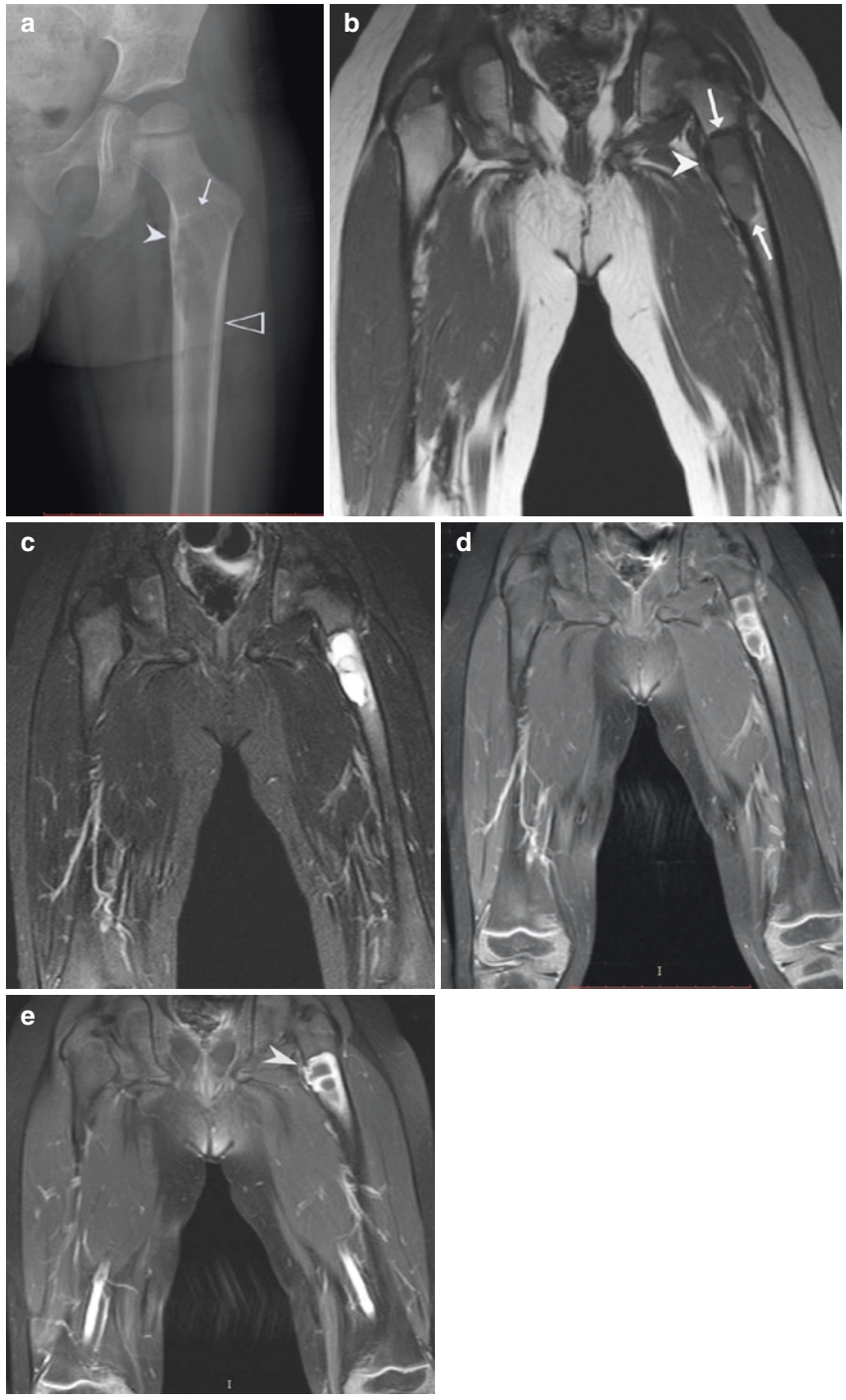

Fig. 31.11 Unicameral bone cyst in a 4-year-old boy with left hip pain after a fall. (**a**) Left femur radiograph shows a well-defined (*arrow*), slightly expanded osteolytic lesion with cortical thickening at the medial cortex (*closed arrowhead*) and solitary periosteal reaction at the lateral aspect of the left femoral proximal metadiaphyseal region (*open arrowhead*). (**b**) Coronal T1-W MR images show a slightly expanded heterogeneously hypointense lesion with well-defined margins (*arrows*) located at the femoral proximal metadiaphyseal region. There is also cortical irregularity at the medial aspect of femoral shaft (*arrowhead*). (**c**) This lesion has heterogeneously hypointense signal with thin septations on the corresponding coronal fat-suppressed T1-W MR image. (**d**, **e**) Contiguous coronal contrast-enhanced fat-suppressed T1-W MR images show septal enhancement. There is also a fracture at the medial cortex (*arrowhead*)

31.10 Aneurysmal Bone Cyst

Aneurysmal bone cyst (ABC) is an intramedullary eccentric metaphyseal and rapidly expansible benign osteolytic lesion with multiloculated blood-filled cystic cavities. There are various forms of ABC: the commonest form is primary ABC which accounts for 70% of cases. The others are secondary ABC (associated with another lesion such as osteoblastoma, chondroblastoma, giant cell tumor, and fibrous dysplasia), solid ABC or giant cell reparative granuloma, and soft tissue ABC. Although ABC may affect any age group, 75–90% of cases occur before the age of 20 years. Although ABC can involve any part of skeleton, long bones with metaphyseal involvement, spine, and pelvis are the most common locations. The distal femur, tibia, humerus, and fibula are the most involved long bones. In the spine, the posterior elements are usually affected.

Radiographs show purely osteolytic, eccentric, aggressive expansile ballooning with a soap bubble pattern, internal trabeculae, and rapid progression, without periosteal reaction. When there is a cortical break, the lesion usually forms a thin sclerotic rim of ossification due to periosteal new bone formation. ABC may cross joints and involve an adjacent bone. CT and MRI are helpful to make differentiation in between ABC and unicameral bone cyst. Although "fluid-fluid" levels were first described in ABC, it can occur in many other lesions such as telangiectatic osteosarcoma (OS), giant cell tumor, chondroblastoma, and metastasis. CT is less sensitive than MRI and reveals a lesion with a thin surrounding shell of bone. A thin shell of soft tissue attenuation, representing the fibrous periosteum, can also been seen (Mascard et al. 2015; Olvi et al. 2015a). CT shows fluid-fluid levels about one-third of lesions. In complex regions, such as the spine and pelvis, CT is helpful to provide a lesion map and planning possible instrumentations. MRI confirms the entirely cystic nature of the lesion, with internal septations and fluid-fluid levels on T2-weighted images. There is enhancement at the cyst walls and internal septae. Primary ABCs have thin septae and minimal or no solid component (Fig. 31.12), whereas secondary ABCs tend to have nodular septae and a larger solid component on MRI. Differential diagnosis includes unicameral bone cyst, giant cell tumor, osteoblastoma, hydatid disease, and telangiectatic OS (Chen et al. 2005; Remotti and Feldman 2012).

Telangiectatic OS was described by Gaylord as a "malignant bone aneurysm" in 1903. This subtype of osteosarcoma is primarily (>90%) composed of multiple aneurysmal dilated cavities that contain blood, with high-grade sarcomatous cells in the peripheral rim and septations around these spaces. Telangiectatic OS may be confused with ABC, both radiologically and pathologically (Remotti and Feldman 2012). MRI demonstrates predominantly signal hyperintensity as well as fluid-fluid levels on T2-weigheted images. Murphey et al. (2003) showed that 52% of cases showed hyperintense signal on T1-weighted images. In telangiectatic OS, there is thick nodular solid tissue surrounding the cystic spaces. This finding is especially prominent after contrast administration (Fig. 31.13). Telangiectatic OS has also a more aggressive growth pattern than ABC, with cortical destruction together with a soft tissue mass (Murphy et al. 2003; Olvi et al. 2015a, b, c, d).

31.11 Juxta-Articular Bone Cyst/ Geode

A juxta-articular bone cyst is an intraosseous nonneoplastic subchondral cystic lesion which is not related to joint pathology. If there is association with degenerative arthritis, the lesion is defined as subchondral pseudocyst or geode which is a well-defined osteolytic lesion adjacent to the periarticular surface. A geode is one of the common differential diagnoses of an osteolytic epiphyseal lesion. This is originally a geological term referring to rounded formations in igneous and sedimentary rocks. Geodes and juxta-articular bone cysts have similar radiological findings except for the presence of osteoarthritis in the former. Geodes can vary in size and are often multiple. Size greater than 2 cm is an unusual finding. On MRI, there is a well-defined round T1-hypointense and T2-hyperintense lesion which may be surrounded by bone marrow

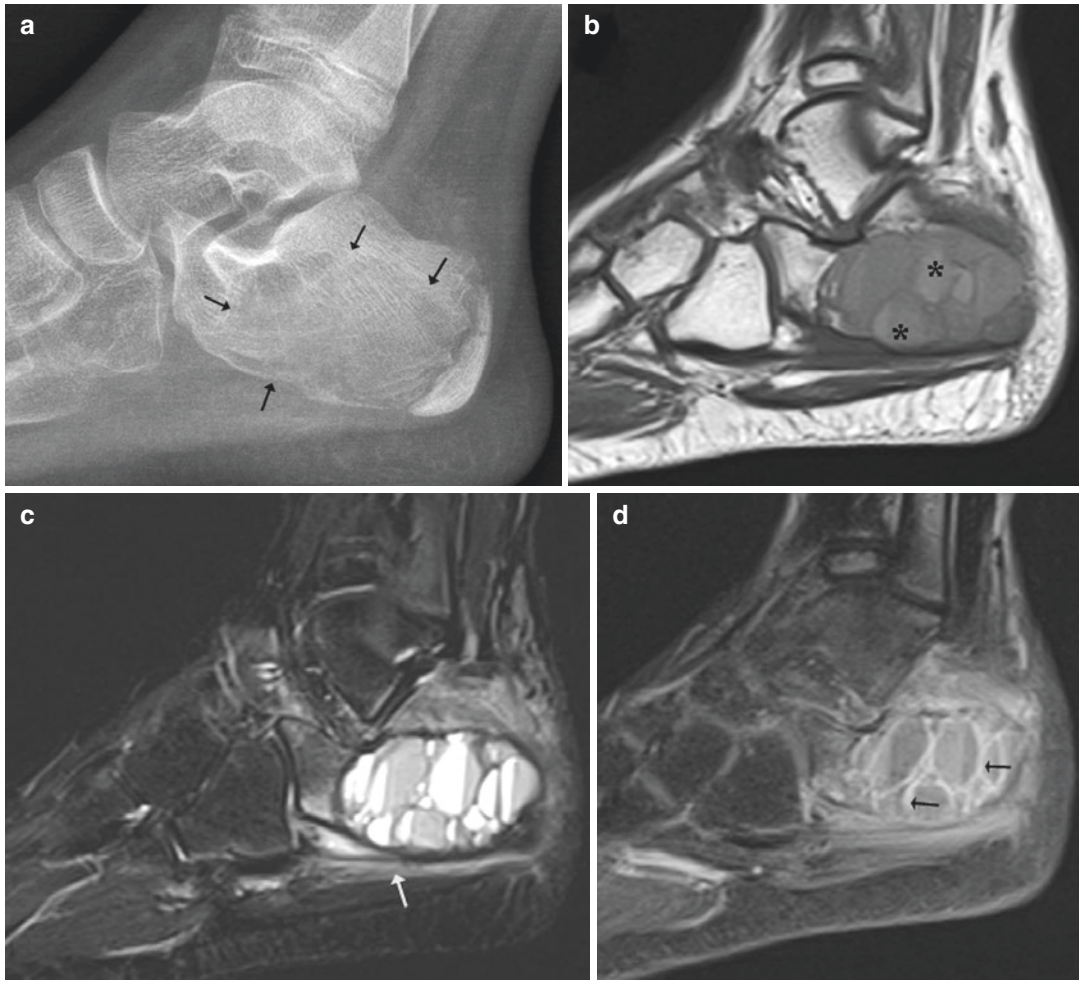

Fig. 31.12 Aneurysmal bone cyst in a 12-year-old boy with left heel pain. (**a**) Lateral radiograph of the left calcaneus shows an osteolytic lesion with loss of bony trabeculation and cortical thinning at the plantar aspect of calcaneus (*arrows*). (**b**) Sagittal T1-W MR image shows a slightly expansile, heterogeneously hypointense lesion within the medullary cavity. The lesion has hypointense well-defined borders and hyperintense blood level components (*black asterisks*). (**c**) The corresponding sagittal STIR MR image shows multiple fluid-fluid levels with thin hypointense septations. The lesion has well-defined hypointense sclerotic margins with minimal soft tissue edema on the plantar aspect of the calcaneus (*arrow*). There is no cortical destruction. (**d**) Thin septal enhancement is seen on sagittal contrast-enhanced fat-suppressed T1-W MR image (*arrows*)

edema and is located in the subchondral bone (Fig. 31.14). Communication of the geode with the joint space is not commonly seen (Arkun and Argin 2014; Olvi et al. 2015c).

31.12 Hydatid Disease

Human echinococcosis is a zoonotic infection. There are four different organisms which may lead to echinococcosis in humans. Hydatid disease (HD), caused by *Echinococcosis granulosus,* is a widespread infestation in the Mediterranean region, Central Asia, South America, South Europe, and Australia. Osseous hydatid disease and muscular hydatidosis are rare, accounting for 0.5–2.5% and 0.5–4%, respectively, of all hydatidosis cases, even in endemic areas. Dogs and other carnivores are definitive hosts; while sheep and other ruminants are intermediate hosts. Humans are secondarily infected by ingestion of food or water contaminated by feces of the dog

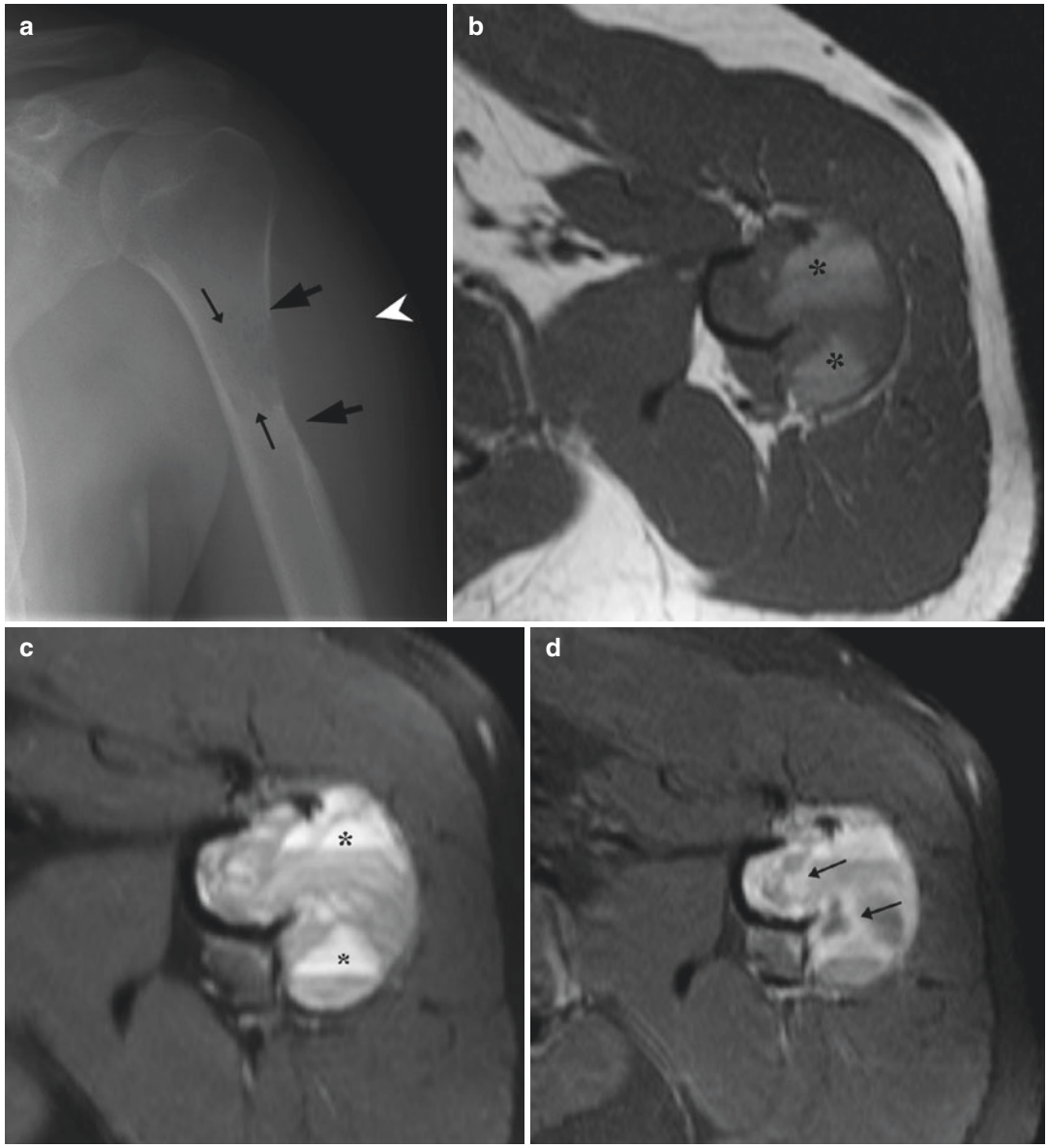

Fig. 31.13 Telangiectatic osteosarcoma in a 25-year-old man with left arm pain and swelling. (**a**) Left humerus radiograph shows an ill-defined intramedullary osteolytic lesion (*thin black arrows*) with cortical destruction (*thick black arrows*) and a soft tissue mass (*white arrowhead*) located at the proximal metaphysic of the humerus. (**b**) Axial T1-W MR image shows an expansile intramedullary bone lesion with cortical destruction. The lesion itself is hypointense with areas of hyperintense signal representing hemorrhage (*black asterisks*). The corresponding (**c**) fat-suppressed T2-W and (**d**) contrast-enhanced fat-suppressed T1-W MR images show multiple fluid-fluid levels and thick irregular septal enhancement (*arrows*)

containing the parasite eggs. After ingestion, the embryos are released from the eggs, transverse the intestinal mucosa, and are disseminated systemically via venous and lymphatic channels. Most of the embryos lodge in the hepatic capillaries, while some pass through capillary sieve and lodge in the lungs and other organs (Polat et al. 2003). Hydatid cyst has three layers, namely, endocyst-germinal layer, ectocyst-laminated membrane, and pericyst. The inner or germinal layer produces the laminated membrane and the scolices that represent the larval stage. Scolices

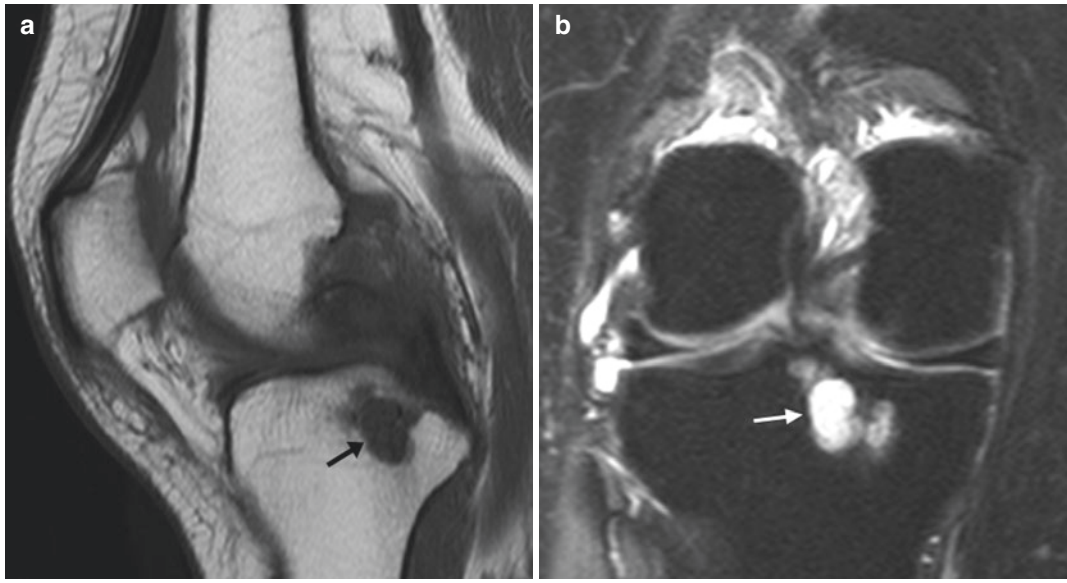

Fig. 31.14 Geode in a 34-year-old woman with right knee pain. (**a**) Sagittal T1-W MR image shows a well-defined hypointense lesion located at the proximal tibial epiphysis (*black arrow*). Posterior cruciate ligament shows thickening with heterogeneous intermediate signal intensity due to myxoid degeneration. (**b**) Coronal fat-suppressed T2-W MR image shows a well-defined, round hyperintense lesion located at the subchondral bone (*white arrow*). Articular cartilage is intact and there is no communication with the joint space

are also produced by the brood capsule, which are small spheres of disrupted germinal membrane. These may remain attached to the germinal membrane, but free-floating brood capsules and scolices form a white sediment known as hydatid sand. Clinically, lesions in bones may present with pain, pathological fracture, secondary infection, deformity, or neurovascular symptoms due to compression (Arkun and Dirim Mete 2011).

Hydatid disease in bones occurs mostly in richly vascularized areas such as vertebrae and long bones. The spine is the most common location, accounting for about 50% of osseous hydatidosis, followed by the pelvis and hip, femur, tibia, ribs, and scapula. Imaging findings are variable, according to stage of the disease. In early stage of the disease, due to microvesicular infiltration into medulla of the bone, embryos reach the medullary cavity. Osteolytic and inflammatory changes without bone expansion occur, which mimics any kind of nonspecific or specific osteomyelitis (e.g., tuberculosis or actinomycosis). Because there are no connective tissue barriers in bone, daughter cysts develop and extend into the bone, with infiltration and replacement of the medulla. Lacking the constraints of this external layer, the cyst progressively enlarges, filling the medullary cavity to a variable extent. Bone erosion and destruction may lead to almost complete osteolysis, bone may distort, and on occasion, its radiological appearance may be confused with ABC, giant cell tumor, myeloma, atypical osteomyelitis, cystic metastases, and fibrous dysplasia. In time, with the erosion of cortex, the lesion extends into the surrounding soft tissues. In the later stage, the disease appears as a well-defined multiloculated osteolytic lesion. Periosteal reaction and sclerosis are uncommon. Direct spread from adjacent skeletal sites such as joint cavity can be seen, especially in juxta-articular lesions.

CT and MRI are useful imaging techniques to show extension of the disease. The CT appearances of bone lesions are similar to those demonstrated on radiographs. However, CT contributes to a better evaluation of extension within the bone, with a clear demarcation of the lesion. MRI provides excellent definition of the lesion size and extension, with its multiplanar imaging capability. On MRI, in case of bone involvement, unilocular or multilocular expansile osteolytic lesion with irregular boundaries shows medium to hyperintense signal on T1-weighted images and hyperintense signal on T2- weighted images. Multiple daughter cysts embedded in a large

cystic lesion also can be detected. Extension of the cyst into adjacent soft tissues and marrow changes are best evaluated with MRI (Figs. 31.15 and 31.16). Bone tumors, tumor-like lesions, and specific and nonspecific infections should be considered in the differential diagnosis. Radiological, laboratory, and clinical findings combined with strong element of suspicion are the key for diagnosis (Arkun 2004; Arkun and Dirim Mete 2011; Ratnaparkhi et al. 2014).

31.13 Hemophilic Pseudotumor

Hemophilia represents a hereditary defect in coagulation. The characteristic clinical presentation of hemophilia is bleeding tendency. Hemophilic pseudotumors are chronic, organized, and encapsulated cystic masses that result from recurrent bleeding in extra-articular musculoskeletal systems. The three forms of pseudotumor are intraosseous, subperiosteal (or cortical),

Fig. 31.15 Hydatid disease in a 40-year-old woman who had incomplete surgery 6 months ago. (**a**) Pelvic radiograph shows a well-defined geographic osteolytic lesion in the right iliac bone (*arrows*). (**b**) Coronal T1-W MR image shows an area of heterogeneous signal hyperintensity with cortical destruction in the right iliac bone (*white arrows*). There is a hypointense irregular mass-like lesion (*black arrowhead*) adjacent to the right superior iliac spine in the subcutaneous fat due to prior operation. (**c**) Coronal STIR MR image shows heterogeneously hyperintense signal changes in the right iliac bone. There is also a round hyperintense soft tissue mass which has central area of signal void adjacent to the medial aspect of the right femoral neck (*white arrow*) and postoperative changes in the right iliopsoas muscle and subcutaneous fat. (**d**) Axial fat-suppressed T2-W MR image shows a daughter cyst in the iliopsoas bursa (*white arrow*) with hyperintense signal

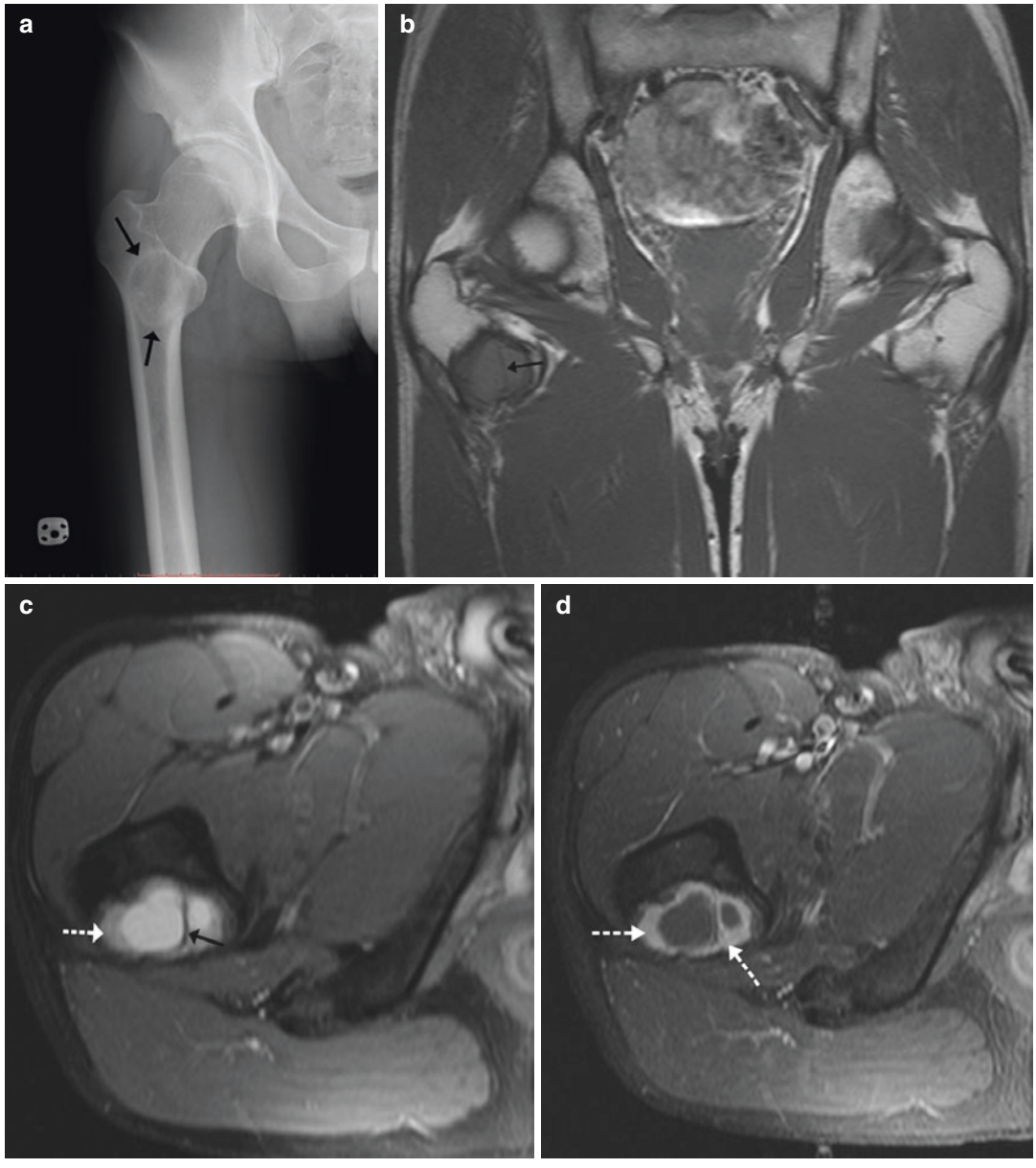

Fig. 31.16 Hydatid disease in a 32-year-old man. (**a**) Right femur radiograph shows a well-defined, slightly osteolytic lesion with sclerotic rim in the lesser trochanter. (**b**) Coronal T1-W MR image shows a tumor-like lesion which has well-defined borders and a hypointense rim in the lesser trochanter of the right femur. There is intermediate signal intensity inside the lesion with thin septae (*arrow*). (**c**) Axial fat-suppressed T2-W MR image shows the multicystic nature of the lesion. The central part of the lesion which is hyperintense with thick hypointense septae (*black arrow*) is surrounded by intermediate signal intensity (*dotted white arrow*). (**d**) The corresponding axial contrast-enhanced fat-suppressed T1-W MR image shows thick peripheral and septal enhancement (*dotted arrows*). This appearance is similar to soft tissue hydatid disease

and soft tissue. The intraosseous form is most common in the femur, pelvic bones, tibia, and hand bones; these lesions can be variably sized. The pseudotumor is usually well demarcated, but it may also be bubbly and destructive. Intraosseous pseudotumors may simulate primary and secondary bone neoplasms (giant cell tumor, desmoplastic fibroma, plasmacytoma, metastasis), tumor-like lesions (unicameral bone cyst, ABC, brown tumor), and even infection or parasitic disease (echinococcosis) because of the pseudotumor's aggressive appearance.

Radiographs, ultrasound imaging, CT, and MRI each play an important role in diagnosis, characterization, and management of pseudotumor. On radiography, intraosseous pseudotumors produce a well-defined, unilobular, or multilobular, expanded osteolytic lesion of variable size. Osseous pseudotumors occur in any portion of the tubular bones, including the metadiaphysis or epiphysis, and have ventral or eccentric epicenters. They may show endosteal scalloping, cortical thinning, or thickening, as well as peripheral sclerosis. Pseudotumors may be quite destructive and completely replace segments of the bone. Repetitive bleeding into soft tissue that is not resolved and replaced by fibrous tissue causes joint contractures and soft tissue pseudotumors.

MRI is the best imaging technique to detect soft tissue pseudotumor. On MRI, a heterogeneous signal in pseudotumors on both T1-weighted and T2-weighted images reflect blood products in various stages of evolution. A peripheral rim of signal hypointensity on all sequences is consistent with the fibrous capsule or hemosiderin (Arkun and Argin 2014) (Fig. 31.17). The diagnosis of an osseous hemophilic pseudotumor relies, in particular, on the knowledge of the underlying bleeding dyscrasia. The radiologist should be aware of the imaging characteristics of this rare complication of hemophilia, in order to avoid misinterpretation of the lesion as a tumoral or infectious

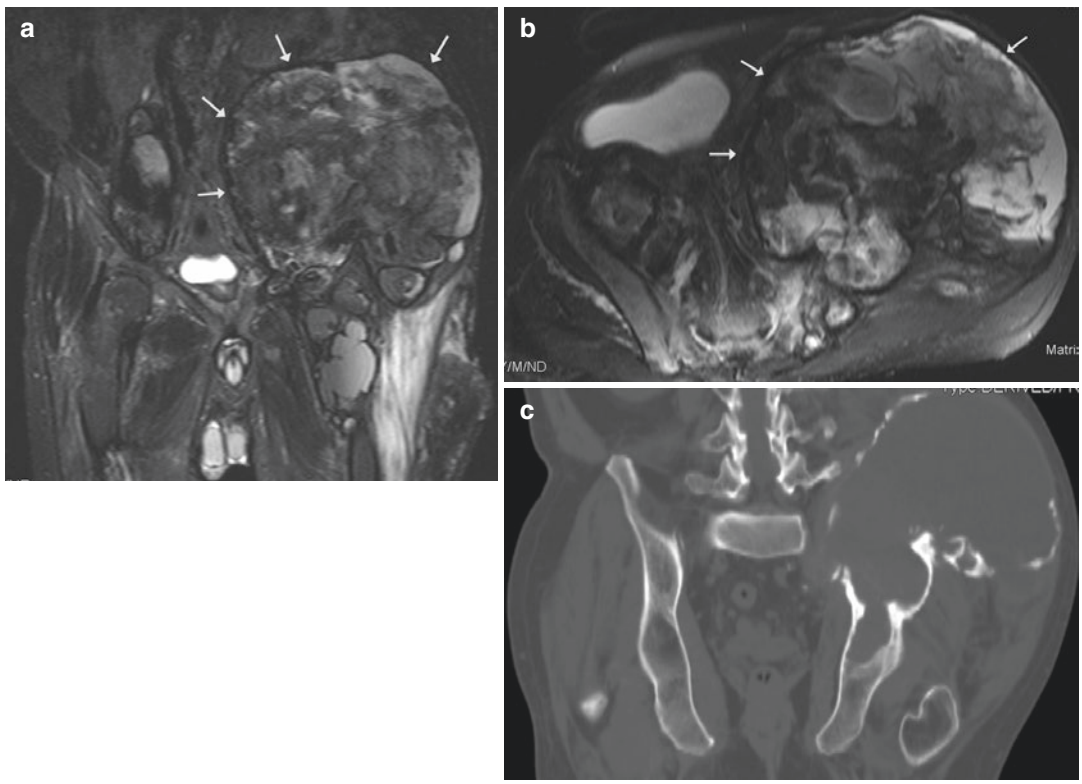

Fig. 31.17 Hemophilic pseudotumor in a 62-year-old man with known hemophilia. (**a**) Coronal and (**b**) axial STIR MR images show a large expansile lesion in the left iliac bone. This lesion has heterogeneous signal intensity with peripheral hypointense rim (*arrows*). (**c**) Coronal reformatted CT image shows a large expansile osteolytic lesion with cortical thinning

lesion, because of the high risk of a preoperative biopsy. Furthermore, cross-sectional imaging is useful in defining the local extent of the lesions, needed for a safe surgical excision of the lesion (Geyskens et al. 2004).

31.14 Paget Disease

Paget disease (PD) is a chronic disorder that can result in enlarged and misshapen bones. This is due to a disturbance in bone modeling and remodeling, resulting from an increase in osteoblastic and osteoclastic activity. The etiology of the condition remains unproven. The overall prevalence of PD is 3–3.7% and increases with age. Pelvic bones, spine, and femur are the most common locations, and 25% of cases are monostotic. Macroscopically and radiologically, PD goes through three phases, namely, an initial, often short-lived, osteolytic phase; an intermediate mixed phase; and a subsequent chronic, and usually quiescent, sclerotic phase. These phases may exist in the same bone. PD usually produces specific features on radiographs (Fig. 31.18a). Characteristic radiographical findings such as

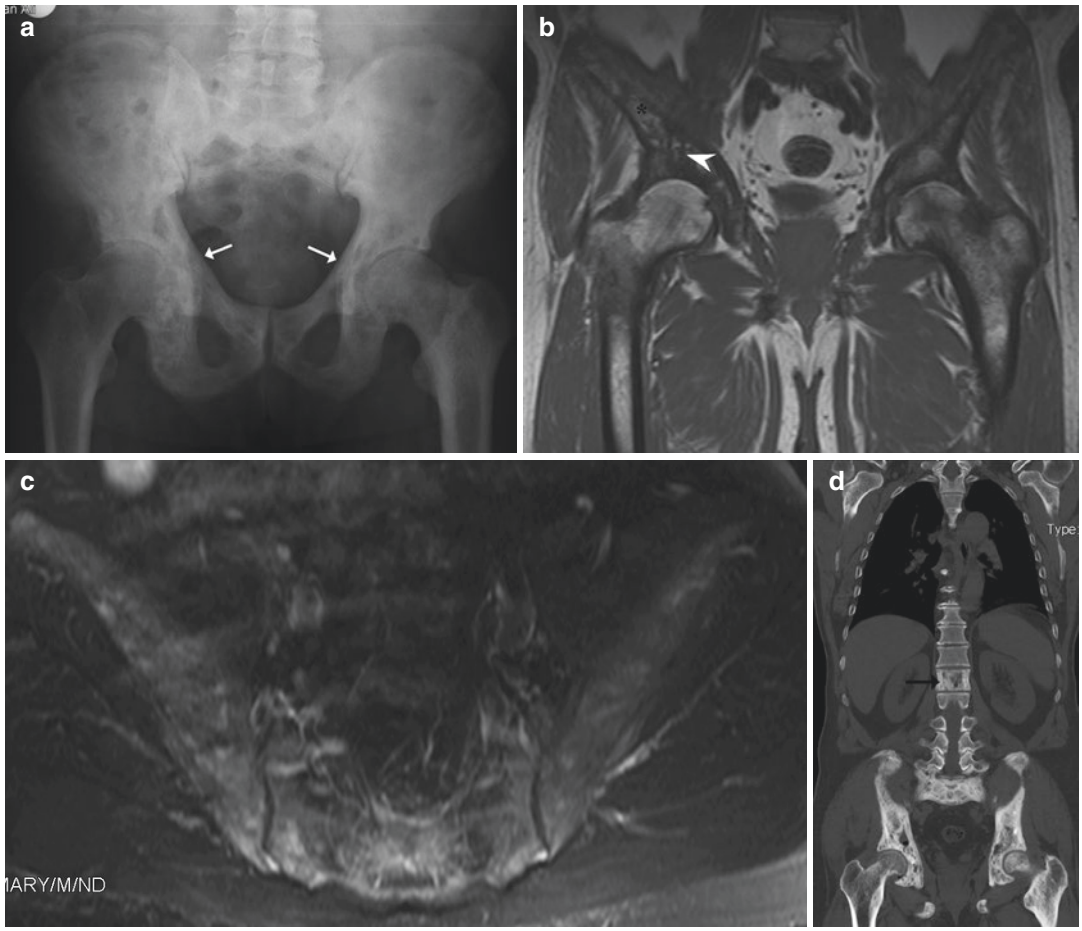

Fig. 31.18 Paget disease in a 67-year-old man. (**a**) Pelvis radiograph shows classical findings of Paget disease such as enlargement of pelvic bones, increased bone density with coarse trabeculation, bilateral hip joint space narrowing, thickening of iliopectineal lines (*arrows*), and heterogeneous increased density in the left femoral head. (**b**) Coronal T1-W MR image shows that the lesion is heterogeneously hypointense with trabecular thickening (*arrowhead*) and maintained yellow marrow (*asterisk*) in the right iliac bone. There is also hypointense signal in the left iliac bone and signal hypointensity with coarse trabeculation in the left femoral head and neck. (**c**) Axial fat-suppressed T2-W MR image shows intermediate and heterogeneous hypointense signal in both iliac bones and sacrum. (**d**) Coronal reformatted CT image shows trabecular coarsening, cortical thickening, and osseous expansion in the pelvic bone. Similar imaging findings are seen in the L1 vertebral body (*arrow*)

bone expansion, coarsened and disorganized trabecular thickening, and splitting of the cortex are seen, except in the initial phase of the disease. On bone scintigraphy, PD produces an increased uptake with characteristic distribution of the disease giving rise to characteristic scintigraphic appearances. However, the polyostotic and atypical monostotic forms of PD can cause confusion in cancer patients (Olvi et al. 2015d; Theodorou et al. 2011).

MRI findings of PD in bone are variable and heterogeneous. Signal intensity depends on the phase of the disease. The most common pattern is dominant signal intensity in pagetic bone similar to that of fat, due to long-standing disease. In the early phase of the disease, there is T1-hypointense signal and T2-hyperintense signal, which probably corresponds to granulation tissue, hypervascularity, and edema. In the late phase, there is signal hypointensity on both T1- and T2-weighted MR images, suggesting the presence of compact bone or fibrous tissue (Fig. 31.18). It should be remembered that PD is a cortical bone disease and the preservation of fatty marrow signal in pagetic bone generally excludes metastatic disease or tumoral infiltration of marrow. There is usually no contrast enhancement in PD disease.

In difficult cases, CT conspicuously exhibits the classic findings of Paget disease that include osteolysis, trabecular coarsening, cortical thickening, and osseous expansion (Whitehouse 2002; Arkun and Argin 2014; Olvi et al. 2015a, b, c, d) (Fig. 31.18d). Soft tissue masses may rarely develop adjacent to Paget disease of bone. These may be due to unmineralized pagetic osteoid, but extraskeletal hematopoiesis has also been described in Paget disease in the paraspinal region. The MRI appearances of parafemoral, parahumeral, and paratibial masses of pagetic osteoid have also been described with a "pseudosarcomatous" appearance. This entity may be misdiagnosed as parosteal osteosarcoma (Whitehouse 2002).

Conclusion

Bone tumors are a relatively infrequent finding in musculoskeletal radiology, and malignant bone tumors are far less common than benign ones. A wide range of musculoskeletal tumors and tumor-like conditions may be encountered when patients undergo radiological examinations. The imaging features of certain normal, reactive, benign, inflammatory, traumatic, and degenerative processes as well as the tumor-like lesions in the musculoskeletal system may mimic malignant tumors. Although MRI is a powerful medical imaging method that has been used extensively in the evaluation of musculoskeletal tumors, non-tumoral or tumor-like lesions can have similar imaging findings. We have reviewed the MRI characteristics of non-tumoral bone lesions which are located in the marrow cavity and cortical bone and which may be misinterpreted as sarcoma. Knowledge of these conditions, combined with recognition of the pattern of abnormal signal intensity and additional clues that may be present on the MRI and correlation with findings from other imaging studies and with the clinical history, frequently helps one narrow the differential diagnosis sufficiently to make the correct diagnosis, or determine whether biopsy is necessary or appropriate.

References

Alyas F, James SL, Davies AM, Saifuddin A (2007) The role of MR imaging in the diagnostic characterisation of appendicular bone tumours and tumour-like conditions. Eur Radiol 17:2675–2686

Antunes C, Graca B, Donato P (2014) Thoracic, abdominal and musculoskeletal involvement in Erdheim-Chester disease: CT, MR and PET imaging findings. Insights Imaging 5:473–482

Arkun R (2004) Parasitic and fungal disease of bones and joints. Semin Musculoskelet Radiol 8:231–242

Arkun R, Dirim Mete B (2011) Musculoskeletal hydatid disease. Semin Musculoskelet Radiol 15:527–540

Arkun R, Argin M (2014) Pitfalls in MR imaging of musculoskeletal tumors. Semin Musculoskelet Radiol 18:63–78

Azouz M, Greenspan A (2005) Melorheostosis. Orphanet Encyclopedia:1–3

Cabarrus MC, Ambekar A, Lu Y, Link TM (2008) MRI and CT of insufficiency fractures of the pelvis and the proximal femur. AJR Am J Roentgenol 191:995–1001

Campbell SE, Fajardo RS (2008) Imaging of stress injuries of the pelvis. Semin Musculoskelet Radiol 12:62–71

Chen LK, Chen HY, Perng HL et al (2005) Imaging features and review literature of aneurysmal bone cyst. Chin J Radiol 30:269–275

Dhondt E, Oudenhoven L, Khan S et al (2006) Nora's lesion, a distinct radiological entity? Skeletal Radiol 35:497–502

Dion E, Graef C, Miquel A et al (2006) Bone involvement in Erdheim-Chester disease: imaging findings including periostitis and partial epiphyseal involvement. Radiology 238:632–639

Eyigor S, Kirazli Y, Memis A, Basdemir G (2005) Erdheim-Chester disease: the effect of bisphosphonate treatment-a case report. Arch Phys Med Rehabil 86:1053–1057

Fayad LM, Kamel IR, Kawamoto S et al (2005) Distinguishing stress fractures from pathologic fractures: a multimodality approach. Skeletal Radiol 34:245–259

Geyskens W, Vanhoenacker FM, van der Zijden T, Peerlinck K (2004) MR imaging of intra-osseous hemophilic pseudotumor: case report and review of the literature. JBR–BTR 87:289–293

Gould CF, Ly JQ, Lattin GE Jr, Beall DP, Sutcliffe JB III (2007) Bone tumor mimics: avoiding misdiagnosis. Curr Probl Diagn Radiol 36:124–141

Howe BM, Johnson GB, Wenger DE (2013) Current concepts in MRI of focal and diffuse malignancy of bone marrow. Semin Musculoskelet Radiol 17:137–144

Hwang S, Panicek DM (2007) Magnetic resonance imaging of bone marrow in oncology, part 1. Skeletal Radiol 36:913–920

Krestan CR, Nemec U, Nemec S (2011) Imaging of insufficiency fractures. Semin Musculoskelet Radiol 15:198–207

Kershen LM, Schucany WG, Gilbert NF (2012) Nora's lesion: bizarre parosteal osteochondromatous proliferation of the tibia. Proc (Bayl Univ Med Cent) 25:369–371

Lyders EM, Whitlow CT, Baker MD, Morris PP (2010) Imaging and treatment of sacral insufficiency fractures. AJNR Am J Neuroradiol 31:201–210

Mascard E, Gomez-Brouchet A, Lambot K (2015) Bone cysts: unicameral and aneurysmal bone cyst. Orthop Traumatol Surg Res 101(1 Suppl):S119–S127

Murphey MD, Jaovisidha S, Temple HT et al (2003) Telangiectatic osteosarcoma: radiologic-pathologic comparison. Radiology 229:545–553

Olvi LG, Lembo GM, Velan O, Santini-Araujo E (2015a) Simple bone cyst. In: Santini-Araujo E, Kalil RK, Bertoni F, Park YK (eds) Tumors and tumor-like lesions of bone, 1st edn. Springer, London

Olvi LG, Gonzalez ML, Santini-Araujo E (2015b) Bizzare parosteal osteochondromatous proliferation. In: Santini-Araujo E, Kalil RK, Bertoni F, Park YK (eds) Tumors and tumor-like lesions of bone, 1st edn. Springer, London

Olvi LG, Lembo GM, Velan O, Santini-Araujo E (2015c) Juxta-articular bone cyst. In: Santini-Araujo E, Kalil RK, Bertoni F, Park YK (eds) Tumors and tumor-like lesions of bone, 1st edn. Springer, London

Olvi LG, Gonzalez ML, Santini-Araujo E (2015d) Paget's disease of bone and sarcoma complicating Paget's disease. In: Santini-Araujo E, Kalil RK, Bertoni F, Park YK (eds) Tumors and tumor -like lesions of bone, 1st edn. Springer-Verlag, London

Polat P, Kantarci M, Alper F, Suma S et al (2003) Hydatid disease from head to toe. Radiographics 23:475–494

Rappaport A, Moermans A, Delvaux S (2014) Nora's lesion or bizarre parosteal osteochondromatous proliferation: a rare and relatively unknown entity. JBR-BTR 97:100–102

Ratnaparkhi CR, Mitra KR, Kulkarni A et al (2014) Primary musculoskeletal hydatid mimicking a neoplasm. J Case Rep 4:424–427

Remotti F, Feldman F (2012) Nonneoplastic lesions that simulate primary tumors of bone. Arch Pathol Lab Med 136:772–788

Smith S, Kransdorf MJ (2000) Primary musculoskeletal tumors of fibrous origin. Semin Musculoskelet Radiol 4:73–88

Stacy GS, Dixon LB (2007) Pitfalls in MR image interpretation prompting referrals to an orthopedic oncology clinic. Radiographics 27:805–828

Stevens MA, El-Khoury GY, Kathol MH, Brandser EA, Chow S (1999) Imaging features of avulsion injury. Radiographics 19:655–672

Suresh S, Muthukumar T, Saifuddin A (2010) Classical and unusual imaging appearances of melorheostosis. Clin Imaging 65:593–600

Theodorou DJ, Theodorou SJ, Kakitsubata Y (2011) Imaging of Paget disease of bone and its musculoskeletal complications: review. AJR Am J Roentgenol 196:S64–S75

Vogler JB III, Murphy WA (1988) Bone marrow imaging. Radiology 168:679–693

Wall J, Feller JF (2006) Imaging of stress fractures in runners. Clin Sports Med 25:781–802

Whitehouse R (2002) Paget's disease of bone. Semin Musculoskelet Radiol 6:313–322